Control of lipid organization and actin assembly during clathrin-mediated endocytosis by the cytoplasmic tail of the rhomboid protein Rbd2

Christa L. Cortesio, Eric B. Lewellyn, and David G. Drubin
Department of Molecular and Cell Biology, University of California, Berkeley, Berkeley, CA 94720

ABSTRACT **Clathrin-mediated endocytosis (CME) is facilitated by a precisely regulated burst of actin assembly. PtdIns(4,5)P2 is an important signaling lipid with conserved roles in CME and actin assembly regulation. Rhomboid family multipass transmembrane proteins regulate diverse cellular processes; however, rhomboid-mediated CME regulation has not been described. We report that yeast lacking the rhomboid protein Rbd2 exhibit accelerated endocytic-site dynamics and premature actin assembly during CME through a PtdIns(4,5)P2-dependent mechanism. Combined genetic and biochemical studies showed that the cytoplasmic tail of Rbd2 binds directly to PtdIns(4,5)P2 and is sufficient for Rbd2's role in actin regulation. Analysis of an Rbd2 mutant with diminished PtdIns(4,5)P2-binding capacity indicates that this interaction is necessary for the temporal regulation of actin assembly during CME. The cytoplasmic tail of Rbd2 appears to modulate PtdIns(4,5)P2 distribution on the cell cortex. The syndapin-like F-BAR protein Bzz1 functions in a pathway with Rbd2 to control the timing of type 1 myosin recruitment and actin polymerization onset during CME. This work reveals that the previously unstudied rhomboid protein Rbd2 functions in vivo at the nexus of three highly conserved processes: lipid regulation, endocytic regulation, and cytoskeletal function.**

Monitoring Editor
Fred Chang
Columbia University

Received: Nov 18, 2014
Revised: Feb 6, 2015
Accepted: Feb 9, 2015

INTRODUCTION

Clathrin-mediated endocytosis (CME) occurs through a well-defined series of events (Weinberg and Drubin, 2012; Merrifield and Kaksonen, 2014). First, endocytic coat proteins and adaptors assemble on the plasma membrane and capture cargo molecules. These early events are followed by recruitment of nucleation-promoting factors (NPFs) and actin-regulatory proteins, which initiate and regulate branched actin network assembly, respectively. A dynamic actin cytoskeleton is essential for plasma membrane invagination in yeast (Kubler and Riezman, 1993; Kaksonen *et al.*, 2003) and facilitates mammalian CME (Yarar *et al.*, 2005; Boulant *et al.*, 2011). Forces generated by polymerizing actin, together with the membrane-bending properties of BAR domain proteins, drive vesicle scission in yeast (Kishimoto *et al.*, 2011).

The actin cytoskeleton plays a central role in CME, and yet the molecular signals and proteins responsible for NPF recruitment and activity regulation have yet to be identified. There are several nucleation-promoting factors (NPFs) that trigger actin polymerization during CME. The most important are the yeast WASP, Las17, and the type 1 myosins, Myo3 and Myo5 (Sun *et al.*, 2006; Galletta *et al.*, 2008). Las17 arrives at endocytic sites with similar timing to the late coat proteins (Kaksonen *et al.*, 2003) and is believed to drive initial Arp2/3-mediated actin polymerization. Las17 NPF activity is important for efficient CME but is not essential due to the NPF activities of the type 1 myosins, Myo3 and Myo5. A burst of actin assembly occurs toward the end of CME, concomitant with the arrival of the myosins, whose NPF activities are critical for efficient membrane invagination. Loss of myosin NPF activity results in a pronounced decrease in productive endocytic events (Sun *et al.*, 2006; Galletta *et al.*, 2008).

Several lines of evidence indicate that the signaling lipid phosphatiylinositol-4,5-bisphosphate (PtdIns(4,5)P2) regulates CME and

This article was published online ahead of print in MBoC in Press (http://www.molbiolcell.org/cgi/doi/10.1091/mbc.E14-11-1540) on February 18, 2015.

C.L.C, E.B.L., and D.G.D. designed the research. C.L.C. and E.B.L. performed experiments. C.L.C. and D.G.D. wrote the article.

Address correspondence to: David G. Drubin (drubin@berkeley.edu).

Abbreviations used: CME, clathrin-mediated endocytosis; GFP, green fluorescent protein; NPFs, nucleation-promoting factors; PtdIns(4,5)P2, phosphatidylinositol 4,5- bisphosphate; RFP, red fluorescent protein; TM, transmembrane; TGN, *trans*-Golgi network.

the actin cytoskeleton in yeast and mammalian cells (Desrivieres *et al.*, 1998; Homma *et al.*, 1998; Yin and Janmey, 2003; Haucke, 2005). Several endocytic proteins contain PtdIns(4,5)P2-binding domains (Haucke, 2005), and PtdIns(4,5)P2 accumulates at endocytic sites (Huang *et al.*, 2004; Sun *et al.*, 2007; Fujita *et al.*, 2009). In yeast, BAR and F-BAR domain–containing proteins such as Syp1, Bzz1, and Rvs161/167 localize to endocytic sites, cluster PtdIns(4,5)P2 (Saarikangas *et al.*, 2009), and can generate extremely stable lipid microdomains (Zhao *et al.*, 2013). In mammalian cells, PtdIns(4,5)P2 depletion is associated with endocytic-site initiation defects (Zoncu *et al.*, 2007; Abe *et al.*, 2008), whereas in yeast, PtdIns(4,5)P2 depletion causes defects in actin organization and endocytic membrane invagination, with only subtle defects in site initiation (Sun and Drubin, 2012).

Large-scale screens in budding yeast identified several physical and genetic interactions between the rhomboid protein Rbd2 and known regulators of CME and the actin cytoskeleton: Las17, Sla1, Bzz1, Lsb3/4, and Rvs161 (Drees *et al.*, 2001; Tong *et al.*, 2002; Costanzo *et al.*, 2010). Rhomboid proteins form a family of transmembrane (TM) proteins consisting of active proteases and catalytically inactive iRhoms (Urban and Dickey, 2011; Adrain and Freeman, 2012). Rhomboid proteins are conserved across all three domains of life (Archaea, Bacteria, and Eukarya) and regulate diverse cellular processes, including intracellular signaling and trafficking events (Koonin *et al.*, 2003). Significant advances in understanding rhomboid proteins biochemically have been made, and yet the cellular functions of several rhomboid proteins remain unknown. Furthermore, research has only scratched the surface of elucidating rhomboid protein regulatory mechanisms, downstream effectors, and functions in vivo.

Budding yeast have two rhomboid proteins, Rbd1 and Rbd2. Rbd1 regulates mitochondrial membrane fusion events (McQuibban *et al.*, 2003), but the function of Rbd2 has remained elusive. In this study, we test the hypothesis that Rbd2 regulates actin polymerization at sites of CME. We demonstrate that through its cytoplasmic tail, Rbd2 regulates the timing of actin assembly at endocytic sites by modulating PtdIns(4,5)P2 and myosin recruitment to endocytic sites. This work reveals an in vivo function in actin regulation during CME for a previously unstudied rhomboid protein.

RESULTS

Actin polymerization initiates prematurely in *rbd2*Δ cells

After several early endocytic proteins, including clathrin and Ede1, appear at endocytic sites for a variable duration, later endocytic proteins such as Las17 and Sla1 arrive, and CME proceeds in a highly predictable and regular manner. After myosin arrival, a burst of actin assembly occurs and generates forces that invaginate the membrane and pinch off vesicles (Weinberg and Drubin, 2012). Perturbations to CME can be sensitively detected by measuring the lifetimes of endocytic proteins. This form of analysis is especially useful for detecting and quantifying effects of mutants that play regulatory roles in the endocytic pathway (Kaksonen *et al.*, 2005; Weinberg and Drubin, 2014).

Several large-scale screens (Drees *et al.*, 2001; Tong *et al.*, 2002; Costanzo *et al.*, 2010) identified genetic and physical interactions between Rbd2 and several actin-regulatory proteins involved in endocytosis (Supplemental Figure S1). We therefore hypothesized that Rbd2 may regulate actin polymerization during CME. We performed simultaneous two-color imaging of endocytic proteins and measured the lifetimes of a coat protein or an early-arriving NPF (Sla1–green fluorescent protein [GFP] or Las17-GFP, respectively), the lifetimes of an actin-associated protein or later-arriving NPF (Sac6–red fluorescent protein [RFP] or Myo5-RFP, respectively), and the time interval between the arrival of either Sla1-GFP or Las17-RFP and either Sac6-RFP or Myo5-RFP at endocytic sites to indicate the onset of actin polymerization in wild-type and *rbd2*Δ cells (Figure 1). We observed that the late, actin-associated proteins (Sac6-RFP or Myo5-RFP) arrived ~7–8 s early relative to the coat protein Sla1-GFP and the early-arriving NPF, Las17-GFP (Figure 1). These observations suggest that initiation of actin polymerization occurs early in *rbd2*Δ cells and therefore that Rbd2 is a negative regulator of actin polymerization, precisely controlling initiation of actin assembly and myosin recruitment during CME. Despite the pronounced effect on the timing of actin assembly initiation, no obvious defect in endocytic uptake of the lipophilic dye FM4-64 was observed in *rbd2*Δ cells (Supplemental Figure S2).

Rbd2 functions in the same pathway as type 1 myosin to regulate actin polymerization during CME

We hypothesized that Rbd2 might function through one of the NPFs, Las17 or Myo3/5, to regulate actin polymerization during CME. The WCA domain of Las17 and the CA domains of Myo3 and Myo5 function to activate Arp2/3-mediated actin polymerization. To test whether Rbd2 absence resulted in premature actin polymerization through Las17 or the myosins, we created an *rbd2*Δ *las17*Δ*WCA* mutant strain and an *rbd2*Δ *myo5*Δ*CA myo3*Δ mutant strain in which Las17 or myosin NPF activity, respectively, is lost. We measured the lifetimes of the coat protein Sla1-GFP and the actin-associated protein Abp1-RFP and the time interval between the arrival of each protein at endocytic sites to indicate the onset of actin polymerization (Figure 2).

As previously reported (Sun *et al.*, 2006), initiation of actin polymerization is delayed in *las17*Δ*WCA* cells based on an increased interval between the arrival of Sla1 and Abp1 (Figure 2A). Combining *rbd2*Δ with the *las17*Δ*WCA* mutant resulted in partial suppression of the *las17*Δ*WCA* endocytic protein lifetime phenotypes, decreasing the interval between Sla1 and Abp1 recruitment (Figure 2A). These data suggest that Rbd2 and Las17 act in parallel pathways (Figure 2A).

Myo3 and Myo5 are very similar in sequence and are believed to have redundant cellular functions (Geli and Riezman, 1996; Goodson *et al.*, 1996). Therefore, to test whether Rbd2 functions in actin polymerization through the myosins, it was necessary to conduct our studies in a *myo3*Δ background, which exhibits apparently normal endocytosis. As expected, patch lifetimes were normal in the *myo3*Δ strain and shorter in *rbd2*Δ *myo3*Δ cells, as reflected in early initiation of actin polymerization, indicated by early Abp1-RFP arrival relative to Sla1-GFP arrival (Figure 2B). Crossing a mutant lacking the Myo5 CA domain into the *myo3*Δ background (*myo5*Δ*CA myo3*Δ) also produced severe phenotypes, with very little patch internalization (Sun *et al.*, 2006). We observed no further effects on patch lifetimes or internalization when *rbd2*Δ *myo5*Δ*CA myo3*Δ cells were examined, suggesting that Rbd2 functions through the same molecular pathway as the myosins, but not Las17, to regulate actin polymerization during CME (Figure 2B).

A subpopulation of Rbd2 is on or near the cell cortex

Rbd2 has five predicted transmembrane domains and a predicted 71–amino acid cytoplasmic C-terminal tail (Figure 3A). We fused GFP to the C-terminus of endogenous Rbd2 and examined its distribution in cells (Figure 3A). Rbd2 was reported to reside primarily but not exclusively in the *cis*-Golgi (Losev *et al.*, 2006). Consistently,

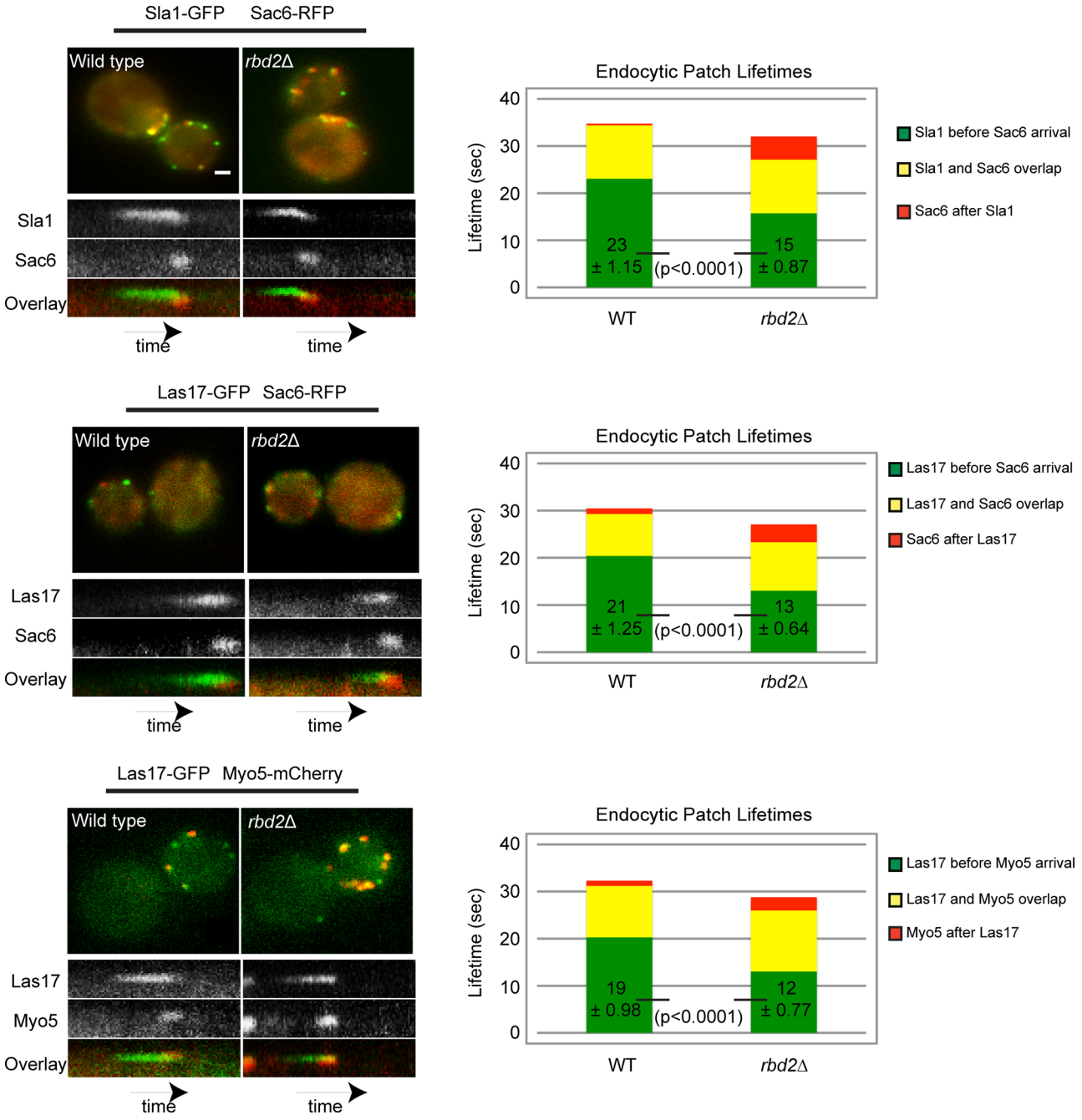

FIGURE 1: Actin initiation and myosin arrival occur prematurely in *rbd2*Δ cells. Simultaneous dual-color images from movies of live wild-type or *rbd2*Δ cells expressing the coat protein Sla1-GFP and the actin-associated protein Sac6-RFP (top), the early-arriving NPF Las17-GFP and the actin-associated protein Sac6-RFP (middle), or the early-arriving NPF Las17-GFP and later- arriving NPF Myo5-mCherry (bottom). Representative kymographs are shown for each. The time elapsed between the arrival of the early-arriving protein and arrival of the later-arriving protein (green and number reported ± SEM), the time of overlap between the two proteins (yellow), and the lifetime of the later protein after the earlier protein (red) disappears were calculated from >100 endocytic events from three independent experiments. The *p* values were calculated using Student's *t* test. Scale bars, 1 μm. Time elapsed for all kymographs, 90 s.

we observed strong colocalization with the early Golgi marker Anp1-RFP (Figure 3B). We also observed colocalization, albeit to a lesser extent, with the *trans*-Golgi network (TGN) marker Sec7-mCherry (Figure 3B). Whereas Rbd2 is primarily localized to bright, internal puncta, a dim subpopulation localizes on or near the cell cortex, as illustrated by kymograph analysis of cells coexpressing Rbd2-GFP and the vesicle soluble *N*-ethylmaleimide–sensitive factor attachment protein receptor RFP-Snc1, which localizes on the plasma membrane (Figure 3C). Rbd2-GFP plasma membrane association was also observed in cells exposed to the lipophilic dye FM4-64 to mark the plasma membrane (Figure 3D), and this signal was enhanced in cells in which CME was effectively blocked by treatment with the actin-depolymerizing drug latrunculin B (Figure 3D).

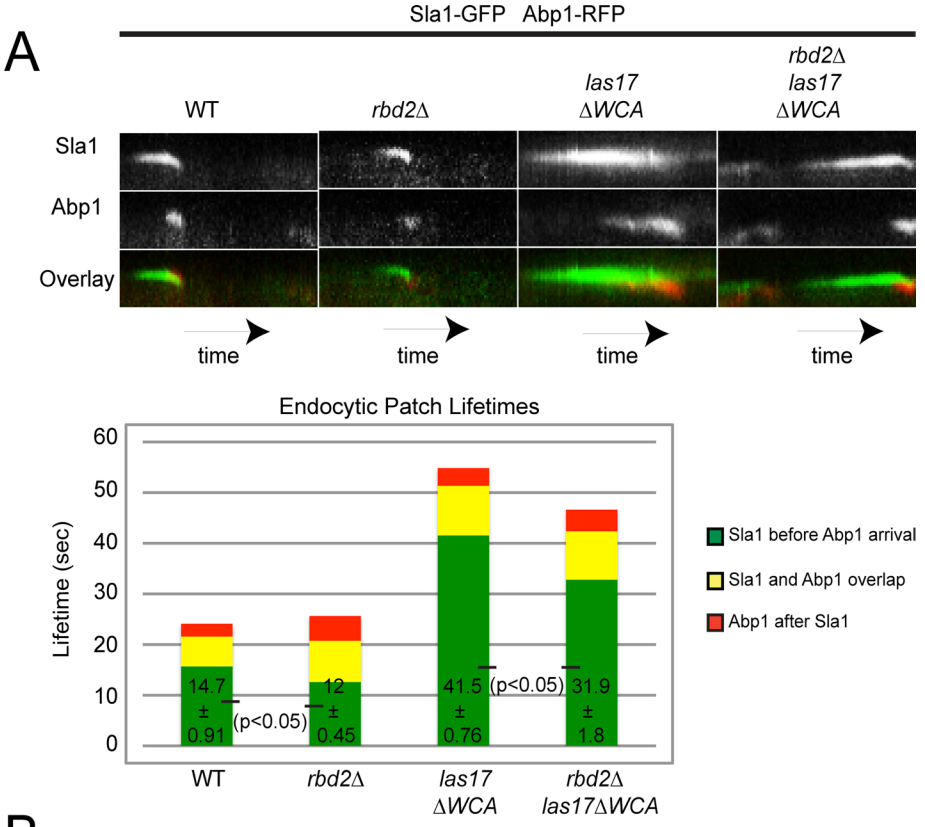

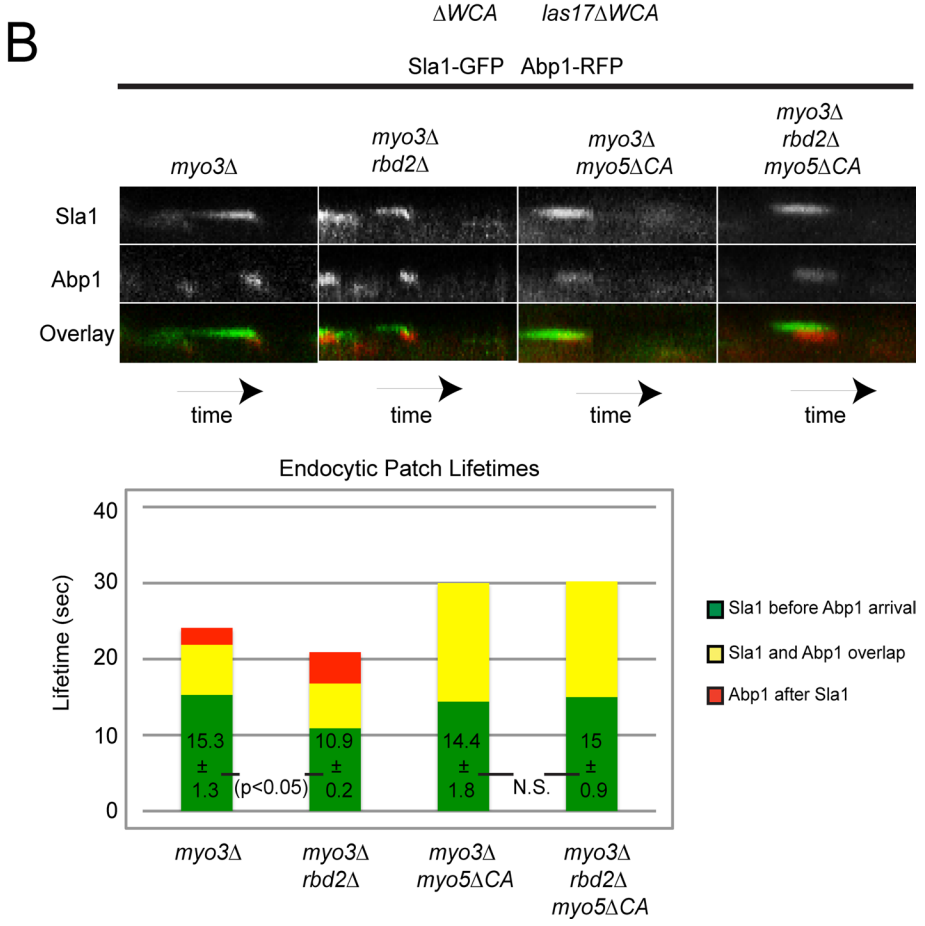

FIGURE 2: Early actin initiation in *rbd2Δ* cells requires the NPF activity of the type 1 myosins but not Las17. Simultaneous dual-color imaging of the coat protein Sla1-GFP and the actin-associated protein Abp1-RFP was performed in (A) wild-type (WT), *rbd2Δ*, *las17ΔWCA*, and *rbd2Δ las17ΔWCA* cells or (B) *myo3Δ*, *rbd2Δ myo3Δ*, *myo3Δmyo5ΔCA*, and *rbd2Δ myo3Δ myo5ΔCA* cells. Representative kymographs are shown for each. The time elapsed between the arrival of Sla1 and Abp1 (green and number reported ± SEM), the time of overlap between the two proteins (yellow), and the lifetime of Abp1 after Sla1 (red) were calculated from >150 endocytic events from four independent experiments. One-way analysis of variance (ANOVA) with a Tukey posttest was used, with $p < 0.05$ considered significant. Scale bars, 1 μm. Time elapsed for all kymographs, 90 s.

To investigate further whether Rbd2 associates with the cell cortex, we performed subcellular fractionation. Using a previously established protocol (Rieder and Emr, 2001), we conducted differential centrifugation on a cell lysate containing epitope-tagged Rbd2 to generate a 13,000 × *g* pellet enriched for vacuoles, plasma membrane, early Golgi, and endoplasmic reticulum (ER). We then performed sucrose gradient fractionation to separate the dense plasma membrane fractions from other organelles (Figure 3E; Rieder and Emr, 2001). In agreement with our imaging data, the majority of Rbd2 was found in fractions enriched for the organelle markers Sec61 (ER), Vps10 (Golgi), Pep12 (Golgi/endosome), and Pho8 (vacuole), which migrated together on our gradient. However, a subpopulation of Rbd2 was present in fractions enriched for the plasma membrane marker Pma1 and not the other organelle markers (Figure 3E). To rule out low levels of organelle contamination in the plasma membrane fractions, we pooled the plasma membrane–enriched fractions in which Sec61, Vsp10, and Pho8 levels were negligible and performed a second sucrose gradient fractionation (Figure 3E). Analysis of fractions from the second fractionation step confirmed the presence of Rbd2 in fractions enriched for the plasma membrane protein Pma1 (Figure 3E). Together the foregoing findings support the conclusion that a population of Rbd2 molecules is associated with the plasma membrane.

The cytoplasmic tail of Rbd2 binds PtdIns(4,5)P2

Several rhomboid proteins possess long cytoplasmic tails for which no functions were known; however, it was predicted that these cytoplasmic regions may contain important trafficking signals (Sheiner *et al.*, 2008). Rbd2 contains an 8-kDa cytoplasmic tail at its C-terminus. We expressed the cytoplasmic tail as the only source of Rbd2 in cells and examined its

cellular localization. The GFP-tagged Rbd2 cytoplasmic tail appeared largely cytosolic, with some enrichment on the cell cortex and other internal membrane structures (Figure 4A). Although only a minor component of plasma membrane, PtdIns(4,5)P2 has a critical role during CME (reviewed in Haucke, 2005). To understand better the biochemical properties of the Rbd2 cytoplasmic tail, we purified affinity-tagged versions (Figure 4B). There are several hydrophobic and charged residues within the cytoplasmic tail that could contribute to phospholipid binding (Figure 4C). To determine whether the Rbd2 cytoplasmic tail binds phospholipids, we used a liposome-binding flotation assay (Ling *et al*., 2012). We found that that purified Rbd2 cytoplasmic tail binds directly and preferentially to liposomes containing PtdIns(4,5)P2 (Figure 4D). The Rbd2 cytoplasmic tail contains three tryptophan residues (Figure 4C). Tryptophan side chains can form hydrogen bonds with lipid head groups and interact with the lipid bilayer through hydrophobic interactions (Schiffer *et al*., 1992). We found that an Rbd2 mutant cytoplasmic tail (W204K) was defective in binding to liposomes containing PtdIns(4,5)P2 (Figure 4D). This result suggests that PtdIns(4,5)P2 binding by Rbd2 is mediated by tryptophan 204 in the cytoplasmic tail.

Rbd2 functions in the same molecular pathway as the PtdIns(4,5)P2- binding F-BAR protein Bzz1 to regulate the actin cytoskeleton during CME

The syndapin-like, F-BAR domain–containing protein Bzz1 localizes to endocytic sites (Soulard *et al*., 2002) and positively regulates actin polymerization in vivo (Arasada and Pollard, 2011) and in vitro (Sun *et al*., 2006). Bzz1 interacts genetically and physically with the type 1 myosins and has been implicated in the recruitment of the actin-polymerizing machinery (Soulard *et al*., 2002). Simultaneous dual-color imaging indicated that Bzz1 arrived ~6 s early relative to the coat protein Sla1-mCherry in *rbd2*Δ cells (Figure 5A). Deletion of *BZZ1* in our yeast strain has no detectable endocytic phenotype (Sun *et al*., 2006). Strikingly, a *bzz1*Δ mutant completely suppressed the endocytic-patch-lifetime phenotype observed in *rbd2*Δ cells (Figure 5B). Furthermore, a PtdIns(4,5)P2-binding mutant of Bzz1, Bzz1R37E (Kishimoto *et al*., 2011), expressed in the *rbd2*Δ strain also suppressed the early-actin-polymerization phenotype (Figure 5B). Taken together, our data provide evidence that Rbd2 functions with Bzz1 to regulate actin through a PtdIns(4,5)P2-dependent mechanism.

Rbd2 regulates PtdIns(4,5)P2 at endocytic sites

A critical role for PtdIns(4,5)P2 during CME is well established (reviewed in Haucke, 2005). In addition, altered PtdIns(4,5)P2 levels and/or distribution also affect actin cytoskeleton organization (Desrivieres *et al*., 1998). Given that several endocytic and actin-regulatory proteins bind PtdIns(4,5)P2-containing lipids or contain putative lipid-binding domains, which may function in their recruitment or activity regulation during CME, and because the cytoplasmic tail of Rbd2 can directly bind to PtdIns(4,5)P2, we hypothesized that the early actin polymerization observed in *rbd2*Δ cells might result from altered PtdIns(4,5)P2 regulation at the plasma membrane. To localize membrane regions enriched in PtdIns(4,5)P2 in cells, we expressed GFP-2XPH-PLCδ in wild-type and *rbd2*Δ cells (Figure 6A). In wild-type cells, we observed a uniform distribution of GFP-2XPH-PLCδ on the plasma membrane, similar to previous reports (Stefan *et al*., 2002; Sun and Drubin, 2012). In contrast, GFP-2XPH-PLCδ appeared in puncta along the plasma membrane in *rbd2*Δ cells, indicating that PtdIns(4,5)P2 organization was dramatically altered (Figure 6A).

To determine whether the PtdIns(4,5)P2 puncta in *rbd2*Δ cells correspond to endocytic sites, we expressed GFP-2XPH-PLCδ in *rbd2*Δ cells expressing the actin-associated, endocytic protein Sac6-RFP (Figure 6B). We found little or no overlap of the PtdIns(4,5)P2 puncta with endocytic sites. Instead, the PtdIns(4,5)P2 puncta often appeared to localize adjacent to endocytic sites and appeared negatively correlated (Figure 6B). Recent work demonstrated that eisosomes function in regulation of PtdIns(4,5)P2 levels on the plasma membrane (Frohlich *et al*., 2014). However, although the PtdIns(4,5)P2 puncta in *rbd2*Δ cells showed limited overlap with the eisosome protein Pil1-mCherry, the overlap was imperfect and not convincingly significant (Figure 6B).

Previous work from our lab demonstrated that the ANTH domain of Sla2 binds specifically to PtdIns(4,5)P2 at endocytic sites and is sufficient for a partial rescue of endocytosis in an *sla2*Δ background (Sun *et al*., 2005, 2007). We used ANTH-GFP as an additional probe to visualize PtdIns(4,5)P2 specifically at sites of endocytosis in control (*sla2*Δ background) and *rbd2*Δ *sla2*Δ cells (Figure 6C). Although ANTH-GFP still appeared at endocytic sites in *rbd2*Δ *sla2*Δ cells, its average lifetime was decreased by almost twofold compared with control cells (Figure 6C), consistent with defective PtdIns(4,5)P2 regulation at endocytic sites. Of interest, expression of the Rbd2 cytoplasmic tail as the only source of Rbd2 caused the ANTH-GFP lifetime to be similar to that observed in the control cells (Figure 6C).

We also detected a genetic interaction between Rbd2 and the ANTH domain of Sla2. Cells expressing ANTH-GFP in an *sla2*Δ background exhibited temperature sensitivity at 37°C. Of interest, this phenotype was suppressed by *rbd2*Δ (Supplemental Figure S3A). Mutation of key lysine residues in the ANTH domain (4K-ANTH) was previously shown to abolish PtdIns(4,5)P2 binding and recruitment to endocytic sites (Sun *et al*., 2007). Cells expressing 4K-ANTH-GFP exhibit severe growth defects and temperature sensitivity (Supplemental Figure S3B). This phenotype could not be suppressed by *rbd2*Δ (Supplemental Figure S3B). Moreover, 4K-ANTH-GFP *rbd2*Δ cell growth was slightly worse than 4K-ANTH-GFP cell growth. This result suggests that suppression of the growth phenotype of ANTH-GFP cells by the *rbd2*Δ mutation occurs through a PtdIns(4,5)P2-dependent mechanism.

Budding yeast have three phosphatidylinositol 5′-phosphatases, known as Sjl1, Sjl2, and Sjl3 (also known as Inp51, Inp52, and Inp53, respectively), which participate in endocytosis and actin function (Singer-Kruger *et al*., 1998). Sjl2 localizes specifically to endocytic sites, and *sjl2*Δ cells exhibit aberrant endocytic protein lifetimes and abnormal actin morphology at endocytic sites due to increased PtdIns(4,5)P2 at endocytic sites (Stefan *et al*., 2005). In further support for a role for Rbd2 in regulation of PtdIns(4,5)P2 at the plasma membrane, we found that *rbd2*Δ partially suppresses the Sac6-RFP lifetime and morphology defects caused by the *sjl2*Δ mutation (Figure 6D). This result suggests that Rbd2 functions in the same molecular pathway as the phosphatidylinositol 5′-phosphatase Sjl2 to regulate actin assembly.

PtdIns(4,5)P2 binding is important for Rbd2-mediated regulation of actin polymerization during CME

We hypothesized that PtdIns(4,5)P2 binding by Rbd2 may be important to regulate actin assembly during CME and decided to test this hypothesis by introducing the W204K mutation into full-length Rbd2 (Figure 7), since the purified W204K cytoplasmic tail is defective in binding to liposomes containing PtdIns(4,5)P2 (Figure 4D). Full-length Rbd2-GFP with a W204K mutation indicated equal expression to wild-type Rbd2 (Figure 7A). Intriguingly, simultaneous dual-color imaging indicated that initiation of actin polymerization occurs

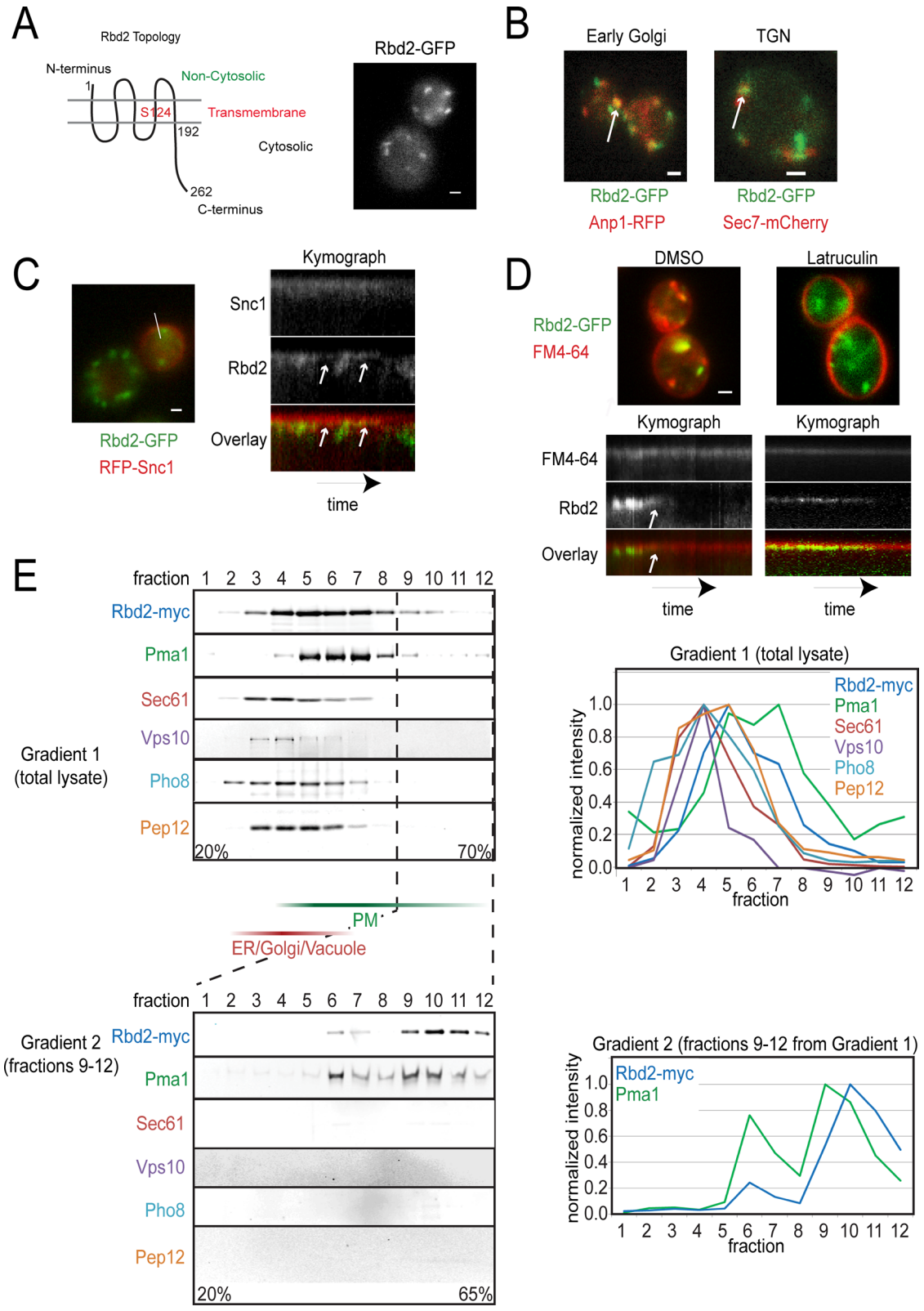

FIGURE 3: A subset of Rbd2 molecules associates with the cell cortex. (A) Predicted Rbd2 topology based on Phobius (Kall *et al.*, 2004). The putative catalytic serine is shown in red in the fourth TM segment. Right, a single frame from a live-cell movie of wild-type cells expressing Rbd2-GFP. (B) Single frame from live-cell movies of cells expressing Rbd2-GFP and the *cis*-Golgi protein Anp1-RFP (left) or the TGN protein Sec7-mCherry (right). White arrows point to areas of colocalization. (C) Single frame from a live-cell movie of a cell expressing Rbd2-GFP and RFP-Snc1. Right, representative kymograph. White arrows point to areas containing a dim signal of Rbd2-GFP that appears to colocalize with Snc1 on the cell cortex. (D) Single frames from live-cell movies of cells expressing Rbd2-GFP and incubated with the lipophilic dye FM4-64 after treatment with vehicle (dimethyl sulfoxide) or latrunculin B. Representative kymographs

~7–8 s early in cells expressing Rbd2 W204K compared with wild-type cells, as indicated by the early arrival of Sac6-RFP relative to Sla1-GFP arrival (Figure 7B). PtdIns(4,5)P2 distribution and dynamics on the plasma membrane and at endocytic sites were also altered in the Rbd2 W204K mutant cells, as revealed by imaging of GFP-2XPH-PLCδ and ANTH-GFP PtdIns(4,5)P2 probes (Figure 7, C and D), respectively. These various phenotypes are similar to the actin- and PtdIns(4,5)P2-related phenotypes observed in *rbd2*Δ cells. Taken together, these data suggest that Rbd2 negatively regulates actin polymerization through a mechanism dependent on the capacity to bind to PtdIns(4,5)P2-containing membranes.

The Rbd2 cytoplasmic tail is sufficient to suppress the early-actin polymerization phenotype in *rbd2*Δ cells

Strikingly, when a hemagglutinin (HA)-tagged Rbd2 cytoplasmic tail was expressed from the endogenous Rbd2 locus, simultaneous dual-color imaging of the coat protein Sla1-GFP and the late, actin-associated protein Sac6-RFP indicated that the early-actin-polymerization phenotype observed in *rbd2*Δ cells was suppressed (Figure 8). These data indicate that the Rbd2 cytoplasmic tail is sufficient to negatively regulate initiation of actin polymerization during CME.

DISCUSSION

A dynamic actin cytoskeleton is important for membrane remodeling and invagination during CME. Although great progress has been made in the identification of proteins that localize to and regulate CME in both yeast and mammals, many unanswered questions remain regarding how endocytic proteins are recruited to endocytic sites and how their activity is regulated. In this study, we identified a role for the rhomboid protein Rbd2 as a negative regulator of actin assembly during CME in budding yeast. Our data suggest that Rbd2, which primarily resides in the Golgi, traffics to or near the cell cortex, where it binds PtdIns(4,5)P2 through its cytoplasmic tail and regulates lipid domain composition and/or organization on the plasma membrane. Using genetics and live-cell imaging, we showed that Rbd2 functions in the same molecular pathway as type 1 myosin, Bzz1, and the lipid phosphatase Sjl2 to regulate the timing of actin polymerization at endocytic sites. Taken together, our results are consistent with a model in which Rbd2 is a regulator of lipid domains on the plasma membrane, which contribute to spatial and temporal regulation of actin assembly during CME.

The Rbd2 cytoplasmic tail is sufficient for temporal regulation of actin initiation during CME through a PtdIns(4,5)P2-dependent mechanism

The results presented here implicate the cytoplasmic, C-terminal tail of Rbd2 as a regulator of PtdIns(4,5)P2 lipid domains on the plasma membrane, which spatially and temporally regulate actin assembly during CME. Rbd2 is a predicted rhomboid protease. However, the 8-kDa Rbd2 cytoplasmic tail, which does not contain the elements necessary for proteolytic activity, was sufficient to suppress the early-actin-polymerization phenotype observed in *rbd2*Δ cells. Thus Rbd2 appears to have multiple functional domains with distinct activities. We focused our studies on activities of the cytoplasmic tail.

A single point mutation (W204K) in full-length Rbd2 that diminished the ability of Rbd2 to bind PtdIns(4,5)P2-containing membranes caused an early-actin-polymerization phenotype similar to that observed in *rbd2*Δ cells. This result indicates that Rbd2-mediated regulation of actin assembly during CME is likely mediated through effects of its cytoplasmic tail on lipid organization, specifically for PtdIns(4,5)P2. This is the first study to identify a cellular role for Rbd2 and implicate the cytoplasmic tail of a rhomboid protein in a specific biological function. Several other rhomboid proteins contain cytoplasmic tails of variable length. The biological roles of these tails remain to be identified (Brooks and Lemieux, 2013). It has been proposed that these tails harbor sorting signals that direct rhomboid proteins to the correct cellular compartment (Sheiner *et al.*, 2008) or regulate rhomboid protease activity by changing active-site accessibility within the membrane bilayer (Del Rio *et al.*, 2007).

Rbd2 functions in the same molecular pathway as myosin, Bzz1, and Sjl2 to regulate initiation of actin assembly during CME

Our data indicate that Rbd2 regulates initiation of actin assembly at endocytic sites through the type 1 myosins and not through yeast WASP. Early myosin recruitment in *rbd2*Δ cells might occur through a PtdIns(4,5)P2-dependent mechanism. PtdIns(4,5)P2 is an established regulator of actin assembly and endocytosis from yeast to mammals. There is precedent for PtdIns(4,5)P2-mediated recruitment of myosin to clathrin-coated structures in mammalian cells (Spudich *et al.*, 2007), and the highly conserved tail homology 1 (TH1) of long-tailed, type 1 myosins from several organisms preferentially binds to acidic phospholipids such as PtdIns(4,5)P2 (Fernandez-Golbano *et al.*, 2014; reviewed in Pollard *et al.*, 1991). PtdIns(4,5)P2 levels and organization on the plasma membrane are regulated by several enzymes and PtdIns(4,5)P2- binding proteins. Two different PtdIns(4,5)P2 probes, one general and one that specifically binds to PtdIns(4,5)P2 at endocytic sites, revealed changes in PtdIns(4,5)P2 organization in *rbd2*Δ cells. The general PtdIns(4,5)P2 probe GFP-2XPH-PLCδ identified PtdIns(4,5)P2 puncta rather than a uniform distribution along the plasma membrane in *rbd2*Δ cells. These puncta do not appear to localize at endocytic sites but instead localize randomly along the cell cortex. The PtdIns(4,5)P2-binding domain of Sla2 (ANTH-GFP), which was used as a probe to specifically monitor PtdIns(4,5)P2 at endocytic sites, indicated that PtdIns(4,5)P2 lifetimes are shorter in *rbd2*Δ cells. We speculate that PtdIns(4,5)P2 accumulation or sequestration in puncta adjacent to endocytic sites may limit PtdIns(4,5)P2 availability at endocytic sites in *rbd2*Δ cells. Moreover, purified Rbd2 cytoplasmic tail specifically and directly binds to PtdIns(4,5)P2 in vitro, and expression of the Rbd2 cytoplasmic tail was sufficient to rescue PtdIns(4,5)P2 levels at endocytic sites. We suggest that the altered PtdIns(4,5)P2 at endocytic sites and the premature recruitment of type 1 myosin during CME in *rbd2*Δ cells are connected causally.

are shown below. The white arrow points to an area of dim Rbd2-GFP that appears to localize on the cell cortex in vehicle-treated cells. (E) Two-step, sucrose gradient fractionation of lysates from cells expressing Rbd2-myc. Fractions were analyzed by Western blot using anti-Sec61 (ER marker), anti-Vps10 (Golgi marker), anti-Pep12 (Golgi/endosome marker), and anti-Pho8 (vacuole marker) to identify internal organelles, anti-Pma1 to identify plasma membrane, or anti-myc (Rbd2). The first fractionation was conducted on cell lysate enriched for ER, Golgi, vacuole, and plasma membrane by differential centrifugation (top). Fractions containing internal organelles and plasma membrane are identified in red and green, respectively, under the gradient 1 immune blot. Fractions containing Pma1 but negligible amounts of Sec61, Vps10, and Pho8 (fractions 9–12) were pooled and subjected to a second fractionation step (bottom). Right, quantification of Western blots. Scale bars, 1 µm. Time scale of all kymographs, 90 s.

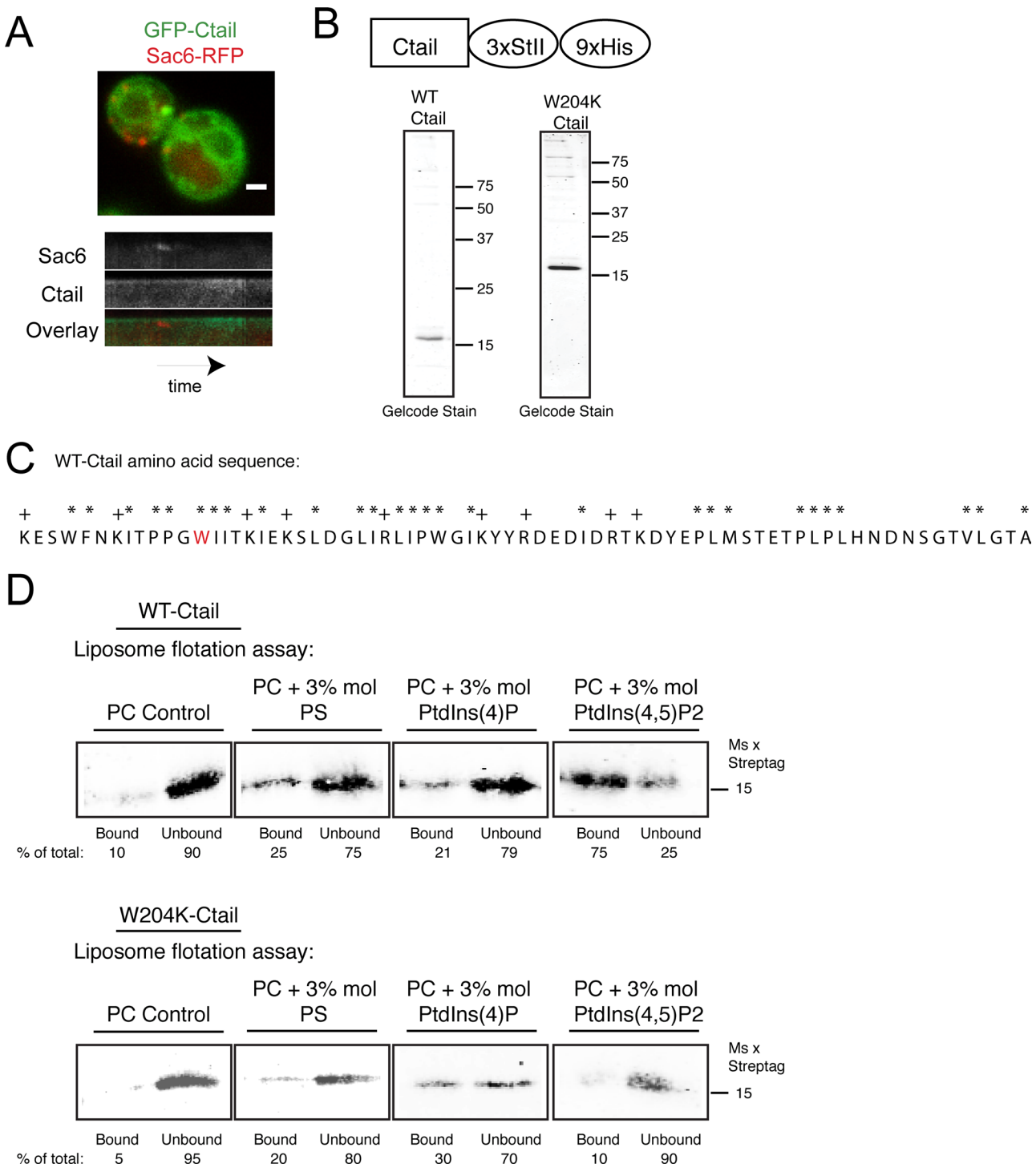

FIGURE 4: Rbd2 binds to PtdIns(4,5)P2 through its cytoplasmic tail. (A) Simultaneous dual-color image from a movie of live cells expressing the Rbd2 GFP-cytoplasmic tail (Ctail) with the actin-associated, endocytic protein Sac6-RFP. A representative kymograph is shown below. (B) Schematic of Rbd2 cytoplasmic tail fusion protein (C-terminal Strep-tag [StII] and histidine [His] tag) used for purification. We stained 1 μg of purified wild-type and W204K cytoplasmic tails using Gelcode Blue. (C) The Rbd2 cytoplasmic tail amino acid sequence, with residue W204 highlighted in red. Residues with potential for lipid/phospholipid binding are denoted with asterisk or plus sign to indicate hydrophobic or charged residue, respectively. (D) The purified proteins (wild-type or W204K cytoplasmic tails) were incubated with PC alone or PC:PS-, PC:PtdIns(4)P-, or PC:PtdIns(4,5)P2-containing liposomes (0.3 mM total lipid and 3% mol PS, PtdIns(4)P, and PtdIns(4,5)P2). Liposomes were separated from unbound protein by flotation assay (see *Materials and Methods*). Fusion protein present in bound or unbound fractions was detected by Western blot using anti–Strep-tag antibody. Protein present in bound and unbound fractions is reported as percentage of the total from a representative experiment performed in triplicate.

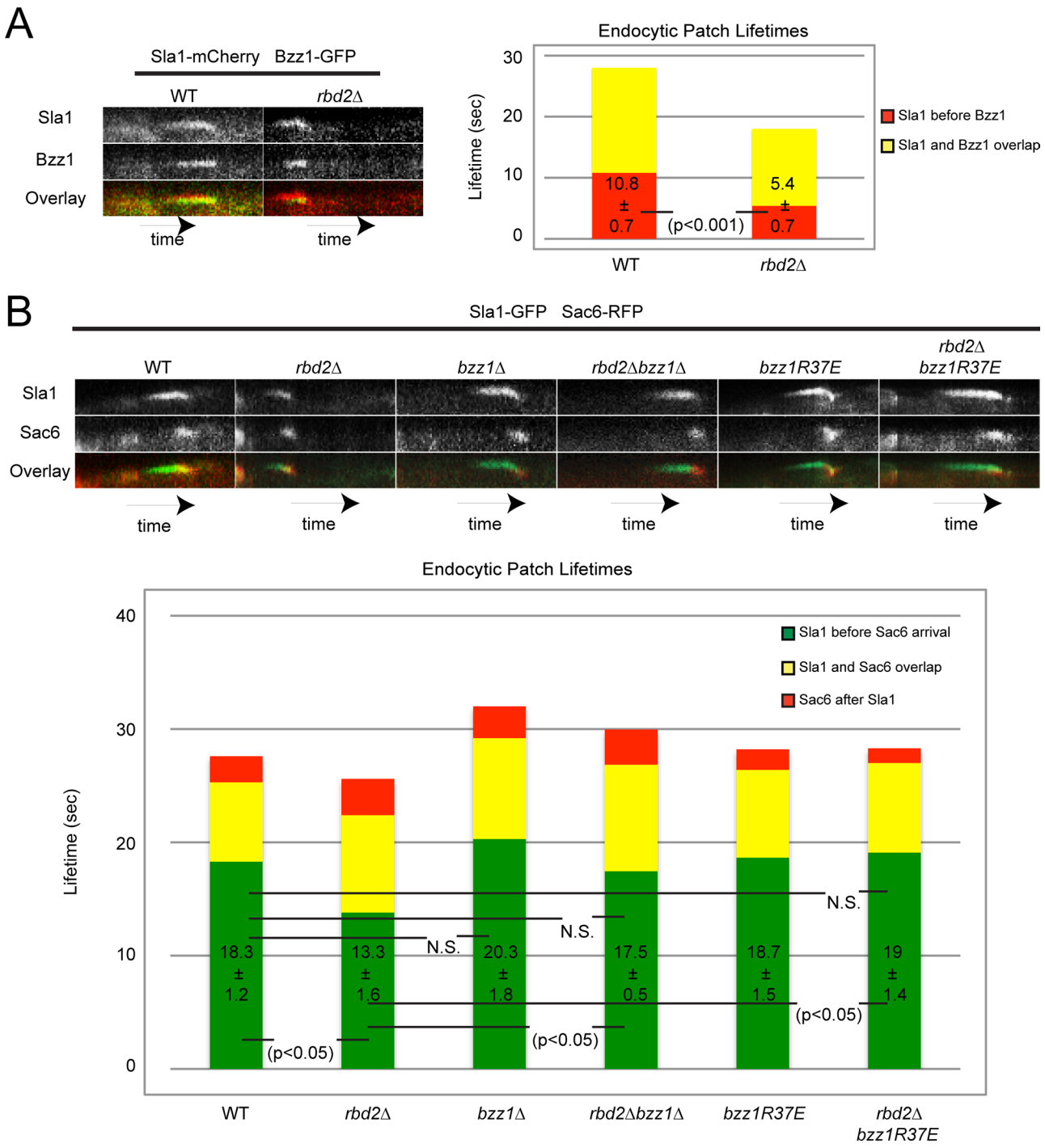

FIGURE 5: Rbd2 functions with Bzz1 to regulate actin assembly during CME. (A) Simultaneous dual-color imaging of the coat protein Sla1-mCherry and the F-BAR domain protein Bzz1-GFP was performed in wild-type or *rbd2*Δ cells. The time elapsed between the arrival of Sla1 (red and number ± SEM) and Bzz1 and the time of overlap between the two proteins (yellow) were calculated from >50 endocytic events from two independent experiments. The *p* values were calculated using Student's *t* test. (B) Simultaneous dual-color imaging of the coat protein Sla1-GFP and the actin-associated protein Sac6-RFP was performed in wild-type (WT), *bzz1*Δ, *rbd2*Δ, *rbd2*Δ *bzz1*Δ, *bzz1R37E*, and *rbd2*Δ *bzz1R37E* cells. The time between the arrival of Sla1 and Sac6 (green and number reported ± SEM), the time of overlap between the two proteins (yellow), and the lifetime of Sac6 after Sla1 (red) were calculated from >100 endocytic events from thee independent experiments. One-way ANOVA with a Tukey posttest was used, with $p < 0.05$ considered significant. Scale bars, 1 μm. Time scale of all kymographs, 90 s.

We acknowledge that our findings of premature myosin recruitment and actin assembly, potentially due to reduced PtdIns(4,5)P2 levels in *rbd2*Δ cells, is somewhat surprising. Severe endocytic lifetime phenotypes have been reported in cells severely depleted for PtdIns(4,5)P2 using an *mss4*^{ts} mutant (Sun *et al.*, 2012). However, how mild to moderate decreases in PtdIns(4,5)P2 affect the early

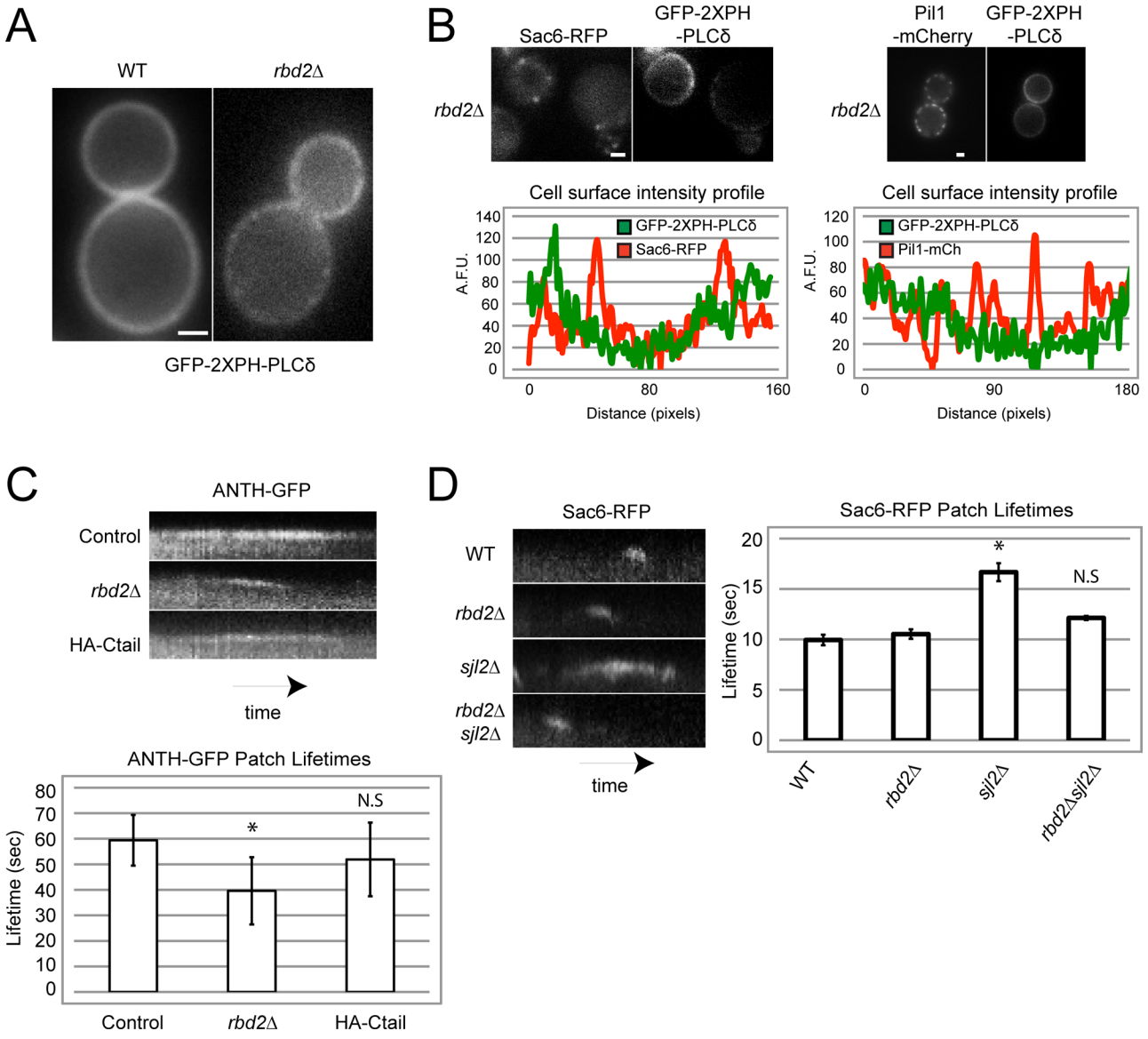

FIGURE 6: Rbd2 regulates PtdIns(4,5)P2 at endocytic sites. (A) Single frame of wild-type or *rbd2*Δ cells expressing the PtdIns(4,5)P2 probe GFP-2XPH-PLCδ from a high-copy plasmid. (B) Single frames of *rbd2*Δ cells expressing Sac6-RFP (left) or Pil1-mCherry (right) and the PtdIns(4,5)P2 probe GFP-2XPH-PLCδ. Representative fluorescence intensity profiles for each protein pair along the cell surface. (C) Lifetime of the PtdIns(4,5)P2 probe ANTH-GFP in *sla2*Δ (Control), *sla2*Δ *rbd2*Δ cells, or *sla2*Δ *rbd2*Δ cells expressing HA-Rbd2 cytoplasmic tail as the only source of Rbd2 was quantified from movies of live cells. Representative kymographs and quantification. *$p < 0.05$ by one-way ANOVA, with a Tukey posttest. (D) Lifetime of Sac6-RFP was measured in WT, *rbd2*Δ, *sjl2*Δ, and *rbd2*Δ*sjl2*Δ cells. Representative kymographs and quantification. *$p < 0.05$ by one-way ANOVA with a Tukey posttest. More than 100 endocytic sites were quantified from three independent experiments. Scale bars, 1 μm. Time scale of all kymographs, 90 s.

stages of endocytic-site maturation and actin assembly is not completely understood. Our study supports a model by which local levels of PtdIns(4,5)P2 are finely regulated by several proteins, including Rbd2, on the cell cortex during CME. Dynamic changes in PtdIns(4,5)P2 concentration and organization likely regulate endocytic protein and actin-regulatory protein recruitment and activity.

Our results suggest that Rbd2 functions in the same molecular pathway as Bzz1 to regulate actin assembly during CME. Bzz1 has been implicated in actin regulation during CME (Sun *et al.*, 2006; Arasada and Pollard, 2011), and its mammalian homologue, syndapin, may also link CME and actin dynamics (Qualmann and Kelly, 2000). Why the *bzz1*Δ mutation suppresses the early actin-polymerization-phenotype of *rbd2*Δ cells is not clear. Part of this uncertainty arises from the fact that *bzz1*Δ has only a very subtle endocytic phenotype in budding yeast (Kishimoto *et al.*, 2011), with no detectable actin phenotypes (Sun *et al.*, 2006). Therefore the in vivo functions of Bzz1 in budding yeast remain somewhat obscure. However, it is known that F-BAR domain–containing proteins like Bzz1 bind and shape PtdIns(4,5)P2-rich membranes at endocytic sites. These proteins form structural platforms to stabilize endocytic sites, recruit downstream effectors, regulate actin nucleation, generate stable lipid domains (Kishimoto *et al.*, 2011; Zhao *et al.*, 2013), and promote vesicle scission during CME (Kishimoto *et al.*, 2011).

Because the actin phenotype was also suppressed in *rbd2*Δ cells by a PtdIns(4,5)P2-binding mutant of Bzz1 (R37E), the relationship between Rbd2 and Bzz1 as it relates to actin regulation depends

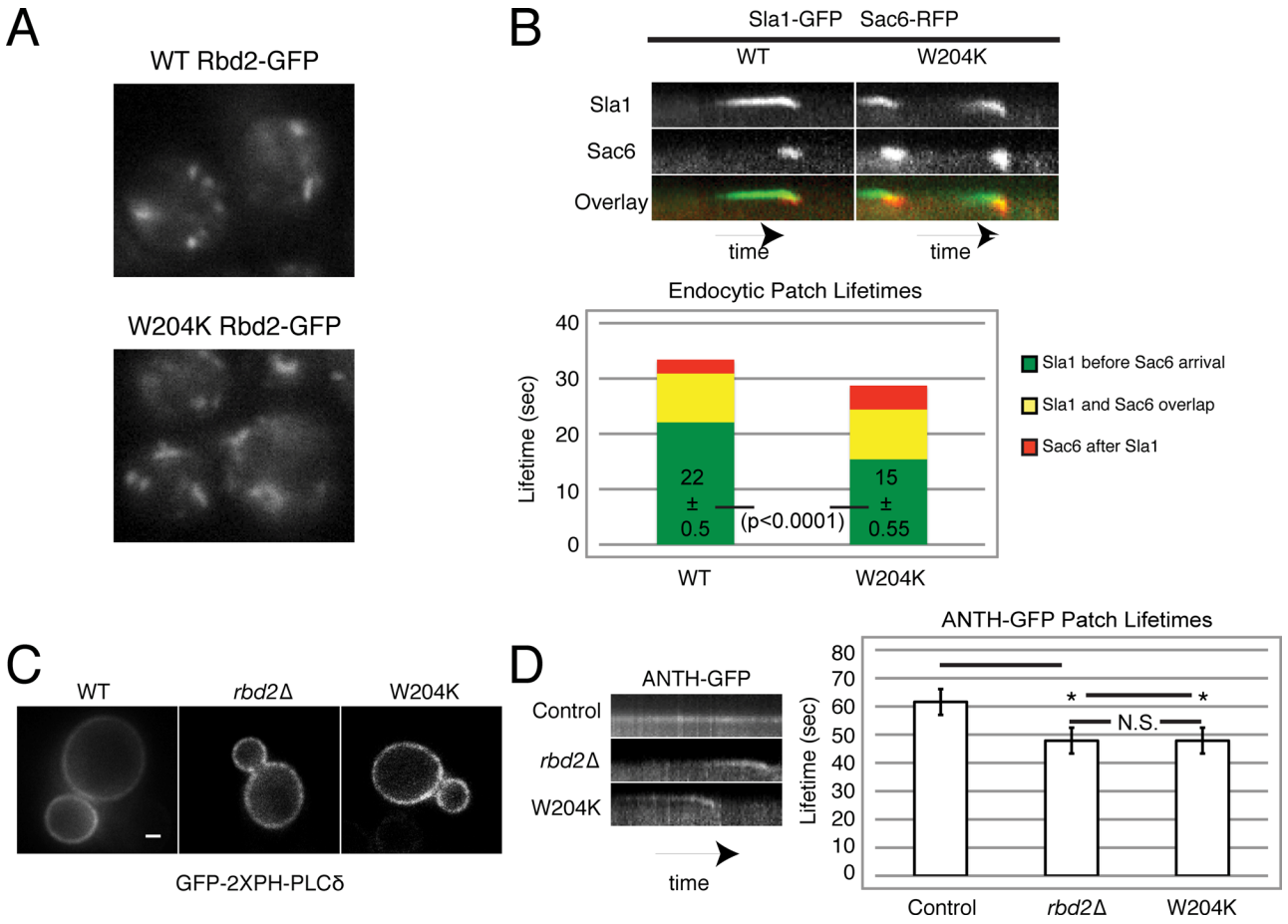

FIGURE 7: An Rbd2 W204K mutant exhibits reduced PtdIns(4,5)P2 binding in vitro and premature actin assembly during CME in vivo. (A) Single frames of cells expressing wild-type Rbd2-GFP and Rbd2 W204K-GFP. (B) Simultaneous dual-color imaging of the coat protein Sla1-GFP and the actin-associated protein Sac6-RFP was performed in wild-type cells or cells expressing full-length Rbd2 W204K as the only source of Rbd2. Representative kymographs. The time elapsed between the arrival of Sla1 and Sac6 (green and number reported ± SEM), the time of overlap between the two proteins (yellow), and the lifetime of Sac6 after Sla1 (red) were calculated from >100 endocytic events from three independent experiments. The *p* value was calculated using Student's *t* test. (C) Images of a wild-type, *rbd2*Δ, and Rbd2 W204K cell expressing the PtdIns(4,5)P2 probe GFP-2XPH-PLCδ from a high-copy plasmid. (D) Lifetime of the PtdIns(4,5)P2 probe ANTH-GFP in *sla2*Δ (control), *sla2*Δ *rbd2*Δ cells, or *sla2*Δ *rbd2*Δ cells expressing Rbd2 W204K as the only source of Rbd2 was quantified from movies of live cells. Representative kymographs and quantification. **p* < 0.05 by one-way ANOVA with a Tukey posttest. N.S., no significance. Scale bars, 1 μm. Time scale of all kymographs, 90 s.

only on the capacity of Bzz1 to bind PtdIns(4,5)P2-containing membranes. It is possible that Rbd2 interacts directly with Bzz1 and that this complex concentrates PtdIns(4,5)P2 at endocytic sites. Indeed, an interaction between Rbd2 and Bzz1 was previously detected in a yeast two-hybrid screen (Tong *et al.*, 2002). Alternatively, Rbd2 might function upstream of the Bzz1 lipid-binding function, in which case Rbd2 and Bzz1 might sequentially regulate PtdIns(4,5)P2 concentration at endocytic sites. Local changes in PtdIns(4,5)P2 as a result of *RBD2* deletion could result in the observed premature Bzz1 recruitment, which then, through a direct or indirect mechanism, might prematurely facilitate myosin recruitment and early initiation of actin polymerization at endocytic sites. If Bzz1 and Rbd2 cooperate to concentrate PtdIns(4,5)P2 at endocytic sites, then local PtdIns(4,5)P2 concentrations would be predicted to be decreased at endocytic sites in *rbd2*Δ cells. This possibility is supported by our observation that the lifetime of the PtdIns(4,5)P2 probe ANTH-GFP is decreased in *rbd2*Δ cells. If Rbd2 is required to concentrate PtdIns(4,5)P2 at endocytic sites, it follows that *RBD2* deletion should suppress mutant phenotypes resulting from increased PtdIns(4,5)P2 at endocytic sites. In agreement with this prediction, *RBD2* deletion suppressed the actin-associated phenotypes of *sjl2*Δ cells, which are defective in PtdIns(4,5)P2 turnover at endocytic sites.

Implications of these findings for understanding rhomboid proteins and actin regulation in more complex eukaryotes

Similar to yeast, actin is also assembled at sites of CME in mammalian cells, in which it facilitates membrane invagination, fission, and vesicle movement (Merrifield *et al.*, 2005; Yarar *et al.*, 2005) and becomes essential under conditions of high membrane tension (Boulant *et al.*, 2011). Both mammalian N-WASP (Galovic *et al.*, 2011) and myosin 1E (Krendel *et al.*, 2007; Cheng *et al.*, 2012) localize to sites of CME in mammalian cells, where they regulate actin assembly. Owing to the high level of conservation of proteins and pathways that regulate actin and CME, it is now important to determine whether a vertebrate Rbd2 homologue exists that similarly regulates lipid domains and actin during CME or other actin-mediated processes. The importance of this goal is underlined by the discovery of rhomboid protein involvement in human disease

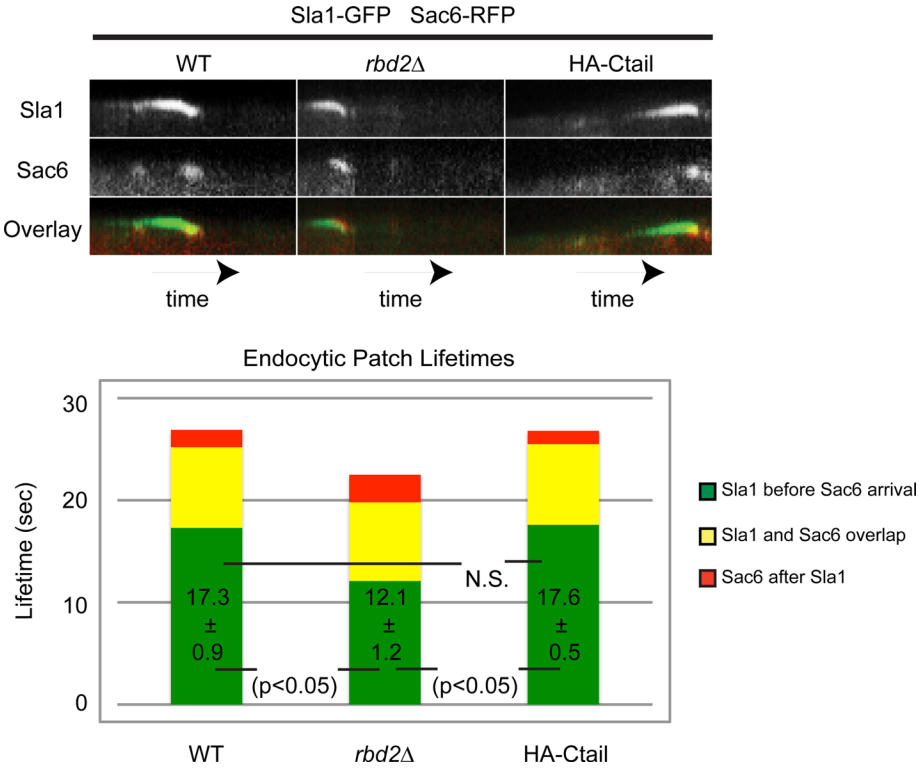

FIGURE 8: The cytoplasmic tail of Rbd2 is sufficient for the regulation of actin initiation. Simultaneous dual-color imaging of the coat protein Sla1-GFP and the actin-associated protein Sac6-RFP was performed in wild-type or *rbd2*Δ cells or cells expressing HA-cytoplasmic tail (Ctail) as the only source of Rbd2. Representative kymographs. The time elapsed between the arrival of Sla1 and Sac6 (green and number reported ± SEM), the time of overlap between the two proteins (yellow) and the lifetime of Sac6 after Sla1 (red) were calculated from >100 endocytic events from three independent experiments. One-way ANOVA with a Tukey posttest was used, with $p < 0.05$ considered significant. Scale bars, 1 μm. Time scale of all kymographs, 90 s.

(reviewed in Urban and Dickey, 2011) and the fact that catalytic rhomboid proteins have unusual enzymatic properties that make them attractive drug targets.

MATERIALS AND METHODS

Plasmids and strains

Yeast strains used in this study are listed in Supplemental Table S1. C-terminal and N-terminal fusions were integrated by homologous recombination as previously described (Longtine *et al.*, 1998; Janke *et al.*, 2004). RBD2 deletion was created by integrating a KanMX6 selection cassette to replace the entire gene open reading frame. Rbd2 W204K was created by QuikChange mutagenesis (forward primer, 5′ GATCACTCCACCAGGAAAAATCATCACCAAAATCG 3′) of pBluescript SK II+ Rbd2 (–500)–(+2600) with a LEU2 cassette inserted at +2104. The resulting Rbd2 W204K was excised from the vector and integrated by homologous recombination. Rbd2 cytoplasmic tail–expressing cells were created by integrating N-terminal GFP or HA tags upstream of residue K192 with a natNT2 selection cassette under the control of the ADH1 promoter (Janke *et al.*, 2004). Correct integration and sequences were verified by PCR and DNA sequencing. The pRS426-GFP-2XPH-PLCδ plasmid was kindly provided by S. Emr (Cornell University, Ithaca, NY).

FM4-64 assay

The dye was solubilized in dimethyl sulfoxide, diluted to 8 μM in synthetic medium, and added to cells. Imaging was performed immediately after addition of the dye at room temperature.

Live-cell imaging

For microscopy, cells were grown in Synthetic Dextrose without tryptophan (to minimize autofluorescence) at 25°C until early log phase. Cells were attached to concanavalin A–coated coverslips, which were sealed to slides with vacuum grease (Dow Corning, Midland, MI). Imaging was done at room temperature using an Olympus IX71, Olympus IX81, or Nikon TE300 equipped with 100×/numerical aperture 1.4 objectives and Orca-100 or Orca II camera (Hamamatsu). Appropriate filter sets and neutral density filters were used during imaging, and images were acquired at rates of 0.5–1 frame/s. Simultaneous two-color imaging was done using an image splitter (Optical Insight) to separate the red and green emission signals to two sides of the camera sensor using 565-nm dichroic mirror and 530/30- and 630/50-nm emission filters. To excite GFP, we used a 488-nm argon-ion laser; for RFP, we used a mercury lamp filtered through a 575/20-nm filter. The excitation beams from these two light sources were combined using a beam splitter. Images of immobilized microbeads that fluoresce at both green and red wavelengths were captured and used to align the cell images. Z-stacks were acquired through the entire cell at 0.2-μm intervals. Images were collected using MetaMorph software (Molecular Devices, Sunnyvale, CA) and processed using ImageJ (National Institutes of Health, Bethesda, MD). Patch lifetimes were calculated from endocytic sites that assembled and disassembled during the movie.

Sucrose gradient fractionation

Yeast organelles were separated using protocols by Rieder and Emr (2001) modified to optimize separation of the plasma membrane from all other organelles. We used a two-step isopycnic centrifugation through sucrose gradients to ensure complete separation of plasma membrane from other organelles. Cells were grown to OD of 0.6 in yeast extract/peptone + 2% dextrose at 30°C. Cells were pelleted, rinsed with water, resuspended in 5 ml of spheroplast buffer containing 50 mM Tris, pH 7.5, 10 mM NaN_3, 40% sucrose, 40 mM 2-mercaptoethanol, and 0.125 mg/ml Zymolyase 100T (Associates of Cape Cod, Cape Cod, MA) and incubated for 30 min at 37°C. Cells were subsequently pelleted at 450 × *g* for 5 min and resuspended in 20 ml of cold lysis buffer containing 20 mM triethanolamine, pH 7.2, 2 mM EDTA, 25% sucrose, and Calbiochem protease inhibitor cocktail IV at 1:500 dilution (EMD-Millipore, Darmstadt, Germany). Cells were subjected to 20 passes in a 40-ml Dounce homogenizer and centrifuged at 500 × *g*. The pellet was resuspended in 20 ml of cold lysis buffer, again subjected to 20 passes in a 40-ml Dounce homogenizer, and centrifuged at 500 × *g*. The supernatants from the first and second rounds were pooled and pelleted at 10,600 rpm for 10 min (~13,000 × *g* at maximum radius) in a type 45 Ti rotor (Beckman Coulter, Brea, CA). The pellet

was gently resuspended in buffer containing 25 mM imidazole, pH 7.0, 2 mM EDTA, and 20% sucrose. The lysate was gently layered on top of a continuous sucrose gradient from 20 to 70% sucrose in 25 mM imidazole, pH 7.0, and 2 mM EDTA. Gradient and resuspension buffer all contained Complete Mini Protease Inhibitor Cocktail (Roche, South San Francisco, CA) at the manufacturer's recommended concentration. The gradient was centrifuged at 45,000 rpm for 16 h in a Beckman SW60 rotor. After the spin, 375-ml fractions were drawn from the top of tube. Fractions 9–12 were shown to contain nearly undetectable signal from the ER marker Sec61, and so these fractions were pooled for subsequent centrifugation in a step gradient. The subsequent gradient was generated by adding 1.0 ml of pooled fractions 9–12, 1.0 ml of 60% sucrose, 1.0 ml of 45% sucrose, 1.0 ml of 33% sucrose, and 0.5 ml of 20% sucrose, all containing 25 mM imidazole, pH 7.0, and 2 mM EDTA. The second gradient was centrifuged for 2 h at 45,000 rpm. Twelve equal fractions were drawn from the top. All fractions from the first and second gradients were analyzed by Western blot analysis. Plasma membrane marker Pma1 was detected using a goat polyclonal antibody yN-20 (Santa Cruz Biotechnology, Dallas, TX), and Rbd2-myc was detected using monoclonal anti-myc 9-E10 antibody. The anti-Sec61, anti-Vps10, anti-Pep12, and anti-Pho8 antibodies were kind gifts from Randy Schekman (University of California, Berkeley, CA).

Purification of Rbd2 cytoplasmic tail

DNA fragments corresponding to Rbd2 amino acids K192–A262 were obtained by PCR amplification of yeast genomic DNA, and a starting M was added. The fragment was cloned into the yeast expression vector p634-Pgal1-StreptagII-9xHIS and transformed into the D1074 yeast strain (kindly provided by D. D'Amours, IRC, University of Montreal, Canada), where the *RBD2* gene was deleted (DDY 4718). The overexpression yeast strain and plasmid were previously described (St-Pierre *et al.*, 2009; Roy *et al.*, 2011). The transformants were induced for 5 h and harvested as previously described (Rodal *et al.*, 2003). Cells were ground using a 6870 Freezer/Mill for six cycles of 3 min of beating, followed by 1 min of cooling (SPEX SamplePrep, Metuchen, NJ).

To purify the Rbd2 cytoplasmic tail, cell powder was thawed in buffer A (50 mM 4-(2-hydroxyethyl)-1-piperazineethanesulfonic acid [HEPES], pH 7.5, 1 M KCl, 0.1% Tween, 20 mM imidazole, and protease inhibitors). The lysate was centrifuged for 20 min at 80,000 rpm, and the cleared supernatant was incubated with nickel-nitriloacetic acid (Qiagen, Valencia, CA) resin for 1 h. The resin was then washed twice with 10 ml of buffer A, and protein was eluted with buffer B (50 mM HEPES, pH 7.5, 1 M KCl, 0.5 M imidazole). The resulting eluate was dialyzed into 50 mM HEPES, pH 7.5, 100 mM KCl, and 5% glycerol and flash frozen in liquid N_2.

Liposome flotation assay

For liposome flotation assays, 97% phosphatidylcholine (PC):3% phosphatidylserine (PS), PtdIns(4)P, or PtdIns(4,5)P2 (Avanti Polar Lipids, Alabaster, AL) liposomes were generated as described previously (Ling *et al.*, 2012) and rehydrated in 50 mM HEPES, pH 7.5, and 100 mM KCl. To create unilamellar liposomes, the liposomes were sonicated for 5 min at room temperature in a water bath. Liposomes (1.2 mM) were then mixed with an equal volume of Rbd2 cytoplasmic tail (resulting in 0.8 µM protein and 0.6 mM final lipid concentration) and incubated for 30 min at room temperature. Samples were then resuspended in 200 µl of buffer (50 mM HEPES, pH 7.5, 100 mM KCl) containing OptiPrep density gradient medium (Sigma-Aldrich, St. Louis, MO) and pipetted into thick-walled centrifuge tubes. Samples were overlaid with 150 µl of 15% OptiPrep buffer, followed by 50 µl of buffer alone. Samples were centrifuged for 1 h at 55,000 rpm at 10°C in a SW-60 ultracentrifuge rotor (Beckman Coulter) in a desktop ultracentrifuge. The top 200 µl of gradient containing liposomes and bound proteins was collected as the bound fraction, and the bottom 200 µl was collected as the unbound fraction. Samples were resuspended in sample buffer and run on 15% SDS–PAGE gels, and the affinity-tagged Rbd2 cytoplasmic tail was detected by immunoblotting using anti–Strep-tag antibody (Qiagen). The relative amounts of protein in bound and unbound fractions were determined using Odyssey software (LI-COR Biosciences, Lincoln, NE).

Western blotting

Yeast lysates were obtained using standard trichloroacetic acid lysis. For Western blot analysis, equal amounts of yeast cell extracts were loaded onto SDS–PAGE gels and transferred to a nitrocellulose membrane. Western blots were imaged and quantified with an infrared imaging system (Odyssey; LI-COR Biosciences).

ACKNOWLEDGMENTS

C.L.C. was supported by National Institutes of Health postdoctoral fellowship F32 GM097876 and E.B.L. by National Institutes of Health postdoctoral fellowship F32 GM100709. This work was supported by National Institutes of Health Grants R01 GM50399 and R01 GM42759 to D.G.D. We thank Damien d'Amours for sharing DNA plasmid constructs for protein purifications and the laboratory of Randy Schekman for sharing yeast strains, antibodies, and plasmids. We thank Jessica Marks for her help with the lipid biochemistry experiments. We thank Yidi Sun, Alexandre Grassart, Connie Peng, and Yansong Miao for critically reading the manuscript and their helpful comments and suggestions.

REFERENCES

Abe N, Inoue T, Galvez T, Klein L, Meyer T (2008). Dissecting the role of PtdIns(4,5)P2 in endocytosis and recycling of the transferrin receptor. J Cell Sci 121, 1488–1494.

Adrain C, Freeman M (2012). New lives for old: evolution of pseudoenzyme function illustrated by iRhoms. Nat Rev Mol Cell Biol 13, 489–498.

Arasada R, Pollard TD (2011). Distinct roles for F-BAR proteins Cdc15p and Bzz1p in actin polymerization at sites of endocytosis in fission yeast. Curr Biol 21, 1450–1459.

Boulant S, Kural C, Zeeh JC, Ubelmann F, Kirchhausen T (2011). Actin dynamics counteract membrane tension during clathrin-mediated endocytosis. Nat Cell Biol 13, 1124–1131.

Brooks CL, Lemieux MJ (2013). Untangling structure-function relationships in the rhomboid family of intramembrane proteases. Biochim Biophys Acta 1828, 2862–2872.

Cheng J, Grassart A, Drubin DG (2012). Myosin 1E coordinates actin assembly and cargo trafficking during clathrin-mediated endocytosis. Mol Biol Cell 23, 2891–2904.

Costanzo M, Baryshnikova A, Bellay J, Kim Y, Spear ED, Sevier CS, Ding H, Koh JL, Toufighi K, Mostafavi S, *et al.* (2010). The genetic landscape of a cell. Science 327, 425–431.

Del Rio A, Dutta K, Chavez J, Ubarretxena-Belandia I, Ghose R (2007). Solution structure and dynamics of the N-terminal cytosolic domain of rhomboid intramembrane protease from Pseudomonas aeruginosa: insights into a functional role in intramembrane proteolysis. J Mol Biol 365, 109–122.

Desrivieres S, Cooke FT, Parker PJ, Hall MN (1998). MSS4, a phosphatidylinositol-4-phosphate 5-kinase required for organization of the actin cytoskeleton in Saccharomyces cerevisiae. J Biol Chem 273, 15787–15793.

Drees BL, Sundin B, Brazeau E, Caviston JP, Chen GC, Guo W, Kozminski KG, Lau MW, Moskow JJ, Tong A, *et al.* (2001). A protein interaction map for cell polarity development. J Cell Biol 154, 549–571.

Fernandez-Golbano IM, Idrissi FZ, Giblin JP, Grosshans BL, Robles V, Grotsch H, Borras Mdel M, Geli MI (2014). Crosstalk between PI(4,5)P2 and CK2 modulates actin polymerization during endocytic uptake. Dev Cell 30, 746–758.

Frohlich F, Christiano R, Olson DK, Alcazar-Roman A, DeCamilli P, Walther TC (2014). A role for eisosomes in maintenance of plasma membrane phosphoinositide levels. Mol Biol Cell 25, 2797–2806.
Fujita A, Cheng J, Tauchi-Sato K, Takenawa T, Fujimoto T (2009). A distinct pool of phosphatidylinositol 4,5-bisphosphate in caveolae revealed by a nanoscale labeling technique. Proc Natl Acad Sci USA 106, 9256–9261.
Galletta BJ, Chuang DY, Cooper JA (2008). Distinct roles for Arp2/3 regulators in actin assembly and endocytosis. PLoS Biol 6, e1.
Galovic M, Xu D, Areces LB, van der Kammen R, Innocenti M (2011). Interplay between N-WASP and CK2 optimizes clathrin-mediated endocytosis of EGFR. J Cell Sci 124, 2001–2012.
Geli MI, Riezman H (1996). Role of type I myosins in receptor-mediated endocytosis in yeast. Science 272, 533–535.
Goodson HV, Anderson BL, Warrick HM, Pon LA, Spudich JA (1996). Synthetic lethality screen identifies a novel yeast myosin I gene (MYO5): myosin I proteins are required for polarization of the actin cytoskeleton. J Cell Biol 133, 1277–1291.
Haucke V (2005). Phosphoinositide regulation of clathrin-mediated endocytosis. Biochem Soc Trans 33, 1285–1289.
Homma K, Terui S, Minemura M, Qadota H, Anraku Y, Kanaho Y, Ohya Y (1998). Phosphatidylinositol-4-phosphate 5-kinase localized on the plasma membrane is essential for yeast cell morphogenesis. J Biol Chem 273, 15779–15786.
Huang S, Lifshitz L, Patki-Kamath V, Tuft R, Fogarty K, Czech MP (2004). Phosphatidylinositol-4,5-bisphosphate-rich plasma membrane patches organize active zones of endocytosis and ruffling in cultured adipocytes. Mol Cell Biol 24, 9102–9123.
Janke C, Magiera MM, Rathfelder N, Taxis C, Reber S, Maekawa H, Moreno-Borchart A, Doenges G, Schwob E, Schiebel E, Knop M (2004). A versatile toolbox for PCR-based tagging of yeast genes: new fluorescent proteins, more markers and promoter substitution cassettes. Yeast 21, 947–962.
Kaksonen M, Sun Y, Drubin DG (2003). A pathway for association of receptors, adaptors, and actin during endocytic internalization. Cell 115, 475–487.
Kaksonen M, Toret CP, Drubin DG (2005). A modular design for the clathrin- and actin-mediated endocytosis machinery. Cell 123, 305–320.
Kall S, Fagerholm HP, Sarvala J (2004). A combined transmembrane topology and signal peptide prediction method. J Mol Biol 338, 1027–1036.
Kishimoto T, Sun Y, Buser C, Liu J, Michelot A, Drubin DG (2011). Determinants of endocytic membrane geometry, stability, and scission. Proc Natl Acad Sci USA 108, E979–E988.
Koonin EV, Makarova KS, Rogozin IB, Davidovic L, Letellier MC, Pellegrini L (2003). The rhomboids: a nearly ubiquitous family of intramembrane serine proteases that probably evolved by multiple ancient horizontal gene transfers. Genome Biol 4, R19.
Krendel M, Osterweil EK, Mooseker MS (2007). Myosin 1E interacts with synaptojanin-1 and dynamin and is involved in endocytosis. FEBS Lett 581, 644–650.
Kubler E, Riezman H (1993). Actin and fimbrin are required for the internalization step of endocytosis in yeast. EMBO J 12, 2855–2862.
Ling Y, Stefan CJ, Macgurn JA, Audhya A, Emr SD (2012). The dual PH domain protein Opy1 functions as a sensor and modulator of PtdIns(4,5)P(2) synthesis. EMBO J 31, 2882–2894.
Longtine MS, McKenzie A 3rd, Demarini DJ, Shah NG, Wach A, Brachat A, Philippsen P, Pringle JR (1998). Additional modules for versatile and economical PCR-based gene deletion and modification in Saccharomyces cerevisiae. Yeast 14, 953–961.
Losev E, Reinke CA, Jellen J, Strongin DE, Bevis BJ, Glick BS (2006). Golgi maturation visualized in living yeast. Nature 441, 1002–1006.
McQuibban GA, Saurya S, Freeman M (2003). Mitochondrial membrane remodelling regulated by a conserved rhomboid protease. Nature 423, 537–541.
Merrifield CJ, Kaksonen M (2014). Endocytic accessory factors and regulation of clathrin-mediated endocytosis. Cold Spring Harb Perspect Biol 6, a016733.
Merrifield CJ, Perrais D, Zenisek D (2005). Coupling between clathrin-coated-pit invagination, cortactin recruitment, and membrane scission observed in live cells. Cell 121, 593–606.
Pollard TD, Doberstein SK, Zot HG (1991). Myosin-I. Annu Rev Physiol 53, 653–681.
Qualmann B, Kelly RB (2000). Syndapin isoforms participate in receptor-mediated endocytosis and actin organization. J Cell Biol 148, 1047–1062.
Rieder SE, Emr SD (2001). Isolation of subcellular fractions from the yeast Saccharomyces cerevisiae. Curr Protoc Cell Biol Chapter 3, Unit 3.8.
Rodal AA, Manning AL, Goode BL, Drubin DG (2003). Negative regulation of yeast WASp by two SH3 domain-containing proteins. Curr Biol 13, 1000–1008.
Roy MA, Siddiqui N, D'Amours D (2011). Dynamic and selective DNA-binding activity of Smc5, a core component of the Smc5-Smc6 complex. Cell Cycle 10, 690–700.
Saarikangas J, Zhao H, Pykalainen A, Laurinmaki P, Mattila PK, Kinnunen PK, Butcher SJ, Lappalainen P (2009). Molecular mechanisms of membrane deformation by I-BAR domain proteins. Curr Biol 19, 95–107.
Schiffer M, Chang CH, Stevens FJ (1992). The functions of tryptophan residues in membrane proteins. Protein Eng 5, 213–214.
Sheiner L, Dowse TJ, Soldati-Favre D (2008). Identification of trafficking determinants for polytopic rhomboid proteases in Toxoplasma gondii. Traffic 9, 665–677.
Singer-Kruger B, Nemoto Y, Daniell L, Ferro-Novick S, De Camilli P (1998). Synaptojanin family members are implicated in endocytic membrane traffic in yeast. J Cell Sci 111, 3347–3356.
Soulard A, Lechler T, Spiridonov V, Shevchenko A, Li R, Winsor B (2002). Saccharomyces cerevisiae Bzz1p is implicated with type I myosins in actin patch polarization and is able to recruit actin-polymerizing machinery in vitro. Mol Cell Biol 22, 7889–7906.
Spudich G, Chibalina MV, Au JS, Arden SD, Buss F, Kendrick-Jones J (2007). Myosin VI targeting to clathrin-coated structures and dimerization is mediated by binding to Disabled-2 and PtdIns(4,5)P2. Nat Cell Biol 9, 176–183.
Stefan CJ, Audhya A, Emr SD (2002). The yeast synaptojanin-like proteins control the cellular distribution of phosphatidylinositol (4,5)-bisphosphate. Mol Biol Cell 13, 542–557.
Stefan CJ, Padilla SM, Audhya A, Emr SD (2005). The phosphoinositide phosphatase Sjl2 is recruited to cortical actin patches in the control of vesicle formation and fission during endocytosis. Mol Cell Biol 25, 2910–2923.
St-Pierre J, Douziech M, Bazile F, Pascariu M, Bonneil E, Sauve V, Ratsima H, D'Amours D (2009). Polo kinase regulates mitotic chromosome condensation by hyperactivation of condensin DNA supercoiling activity. Mol Cell 34, 416–426.
Sun Y, Carroll S, Kaksonen M, Toshima JY, Drubin DG (2007). PtdIns(4,5)P2 turnover is required for multiple stages during clathrin- and actin-dependent endocytic internalization. J Cell Biol 177, 355–367.
Sun Y, Drubin DG (2012). The functions of anionic phospholipids during clathrin-mediated endocytosis site initiation and vesicle formation. J Cell Sci 125, 6157–6165.
Sun Y, Kaksonen M, Madden DT, Schekman R, Drubin DG (2005). Interaction of Sla2p's ANTH domain with PtdIns(4,5)P2 is important for actin-dependent endocytic internalization. Mol Biol Cell 16, 717–730.
Sun Y, Martin AC, Drubin DG (2006). Endocytic internalization in budding yeast requires coordinated actin nucleation and myosin motor activity. Dev Cell 11, 33–46.
Tong AH, Drees B, Nardelli G, Bader GD, Brannetti B, Castagnoli L, Evangelista M, Ferracuti S, Nelson B, Paoluzi S, *et al.* (2002). A combined experimental and computational strategy to define protein interaction networks for peptide recognition modules. Science 295, 321–324.
Urban S, Dickey SW (2011). The rhomboid protease family: a decade of progress on function and mechanism. Genome Biol 12, 231.
Weinberg J, Drubin DG (2012). Clathrin-mediated endocytosis in budding yeast. Trends Cell Biol 22, 1–13.
Weinberg JS, Drubin DG (2014). Regulation of clathrin-mediated endocytosis by dynamic ubiquitination and deubiquitination. Curr Biol 24, 951–959.
Yarar D, Waterman-Storer CM, Schmid SL (2005). A dynamic actin cytoskeleton functions at multiple stages of clathrin-mediated endocytosis. Mol Biol Cell 16, 964–975.
Yin HL, Janmey PA (2003). Phosphoinositide regulation of the actin cytoskeleton. Annu Rev Physiol 65, 761–789.
Zhao H, Michelot A, Koskela EV, Tkach V, Stamou D, Drubin DG, Lappalainen P (2013). Membrane-sculpting BAR domains generate stable lipid microdomains. Cell Rep 4, 1213–1223.
Zoncu R, Perera RM, Sebastian R, Nakatsu F, Chen H, Balla T, Ayala G, Toomre D, De Camilli PV (2007). Loss of endocytic clathrin-coated pits upon acute depletion of phosphatidylinositol 4,5-bisphosphate. Proc Natl Acad Sci USA 104, 3793–3798.